Journal of Materials Chemistry C

ROYAL SOCIETY OF CHEMISTRY

PAPER

View Article Online
View Journal | View Issue

Cite this: *J. Mater. Chem. C*, 2023, **11**, 13740

Solvatochromic and aggregation-induced emission active nitrophenyl-substituted pyrrolidinone-fused-1,2-azaborine with a pre-twisted molecular geometry†

Albert D. Campbell Jr.,[a] Kaia Ellis,[a] Lyric K. Gordon,[a] Janiyah E. Riley,[a] VuongVy Le,[b] Kimberly K. Hollister,[be] Stephen O. Ajagbe,[c] Samer Gozem,[c] Robert B. Hughley,[a] Adeline M. Boswell,[a] Ophelia Adjei-sah,[a] Prioska D. Baruah,[a] Ra'Nya Malone,[a] Logan M. Whitt,[d] Robert J. Gilliard Jr.[e] and Carl Jacky Saint-Louis *[a]

Received 10th September 2023,
Accepted 12th September 2023

DOI: 10.1039/d3tc03278g

rsc.li/materials-c

Boron–nitrogen-containing heterocycles with extended conjugated π-systems such as polycyclic aromatic 1,2-azaborines, hold the fascination of organic chemists due to their unique optoelectronic properties. However, the majority of polycyclic aromatic 1,2-azaborines aggregate at high concentrations or in the solid-state, resulting in aggregation-caused quenching (ACQ) of emission. This practical limitation poses significant challenges for polycyclic aromatic 1,2-azaborines' use in many applications. Additionally, only a few solvatochromic polycyclic aromatic 1,2-azaborines have been reported and they all display minimal solvatochromism. Therefore, the scope of available polycyclic 1,2-azaborines needs to be expanded to include those displaying fluorescence at high concentration and in the solid-state as well as those that exhibit significant changes in emission intensity in various solvents due to different polarities. To address the ACQ issue, we evaluate the effect of a pre-twisted molecular geometry on the optoelectronic properties of polycyclic aromatic 1,2-azaborines. Specifically, three phenyl-substituted pyrrolidinone-fused 1,2-azaborines (PFAs) with similar structures and functionalized with diverse electronic moieties (–H, $-NO_2$, –CN, referred to as **PFA 1**, **2**, and **3**, respectively) were experimentally and computationally studied. Interestingly, **PFA 2** displays two distinct emission properties: (1) solvatochromism, in which its emission and quantum yields are tunable with respect to solvent polarity, and (2) fluorescence that can be completely "turned off" and "turned on" *via* aggregation-induced emission (AIE). This report provides the first example of a polycyclic aromatic 1,2-azaborine that displays both AIE and solvatochromism properties in a single BN-substituted backbone. According to time-dependent density functional theory (TD-DFT) calculations, the fluorescence properties of **PFA 2** can be explained by the presence of a low-lying n–π* charge transfer state inaccessible to **PFA 1** or **PFA 3**. These findings will help in the design of future polycyclic aromatic 1,2-azaborines that are solvatochromic and AIE-active as well as in understanding how molecular geometry affects these compounds' optoelectronic properties.

[a] *Department of Chemistry and Biochemistry, Kennesaw State University, Kennesaw, GA, 30144, USA. E-mail: csaintlo@kennesaw.edu; Tel: 1-470-578-6048*
[b] *Department of Chemistry, University of Virginia, Charlottesville, VA, 22904, USA*
[c] *Department of Chemistry, Georgia State University, Atlanta, GA, 30302, USA*
[d] *Department of Chemistry & Biochemistry, The University of Alabama, Tuscaloosa, Alabama, 35487, USA*
[e] *Department of Chemistry, Massachusetts Institute of Technology, 77 Massachusetts Avenue, Cambridge, MA, 02139, USA*

† Electronic supplementary information (ESI) available: Experimental section: synthetic protocols, characterizations (^{1}H NMR, ^{13}C{^{1}H} NMR, ^{11}B{^{1}H} NMR, high resolution mass spec, FT-IR spectra), UV-visible spectra of compounds **1–3** in various solvents, solid-state excitation spectra of compounds **1–3**, **benzo-azaborine** and **nitrobenzo-azaborine**, emission spectra of compounds **1–3** in various solvents, solid-state emission spectra of compounds **1–3**, **benzo-azaborine** and **nitrobenzo-azaborine**, and X-ray crystallographic data for **PFA 3**. CCDC 2272026. For ESI and crystallographic data in CIF or other electronic format see DOI: https://doi.org/10.1039/d3tc03278g

Introduction

Polycyclic aromatic hydrocarbons (PAHs) have been extensively studied for potential applications in optoelectrical devices[1–3] due to their unique optical and electronic properties.[4–7] In recent decades, researchers have incorporated various main group elements such as boron, nitrogen, phosphorus or sulfur into the structural backbone of PAHs to investigate their influence on the optical and electronic properties.[8–12] In the late 1950s, Dewar and coworkers incorporated a three coordinated boron into the backbone of a PAH and reported the first singly boron–nitrogen (BN)-substituted aromatic compounds, the 9,10-dihydro-9-aza-10-boraphenanthrene system.[13] These arene isosteres were constructed by replacing a HC═CH (or C═C) bond from a PAH with a HB–NH (or B–N) bond, respectively. Incorporation of a B–N bond into the structural backbone of PAHs has been known to preserve the non-flexible conjugated π-systems and induce modification of the electronic transition energies.[14–22]

Despite a nearly seventy-year gap since Dewar reported the synthesis and characterization of the first singly BN-substituted aromatic compounds, polycyclic aromatic compounds containing the B–N bond have held the fascination of the organic chemistry community due to their potential use in materials[23] and biomedical research.[24] For example, in the past two decades, researchers have focused their efforts on improving electroluminescent (EL) devices[25–27] by pursuing BN-substituted polycyclic aromatic compounds that exhibit new and/or enhanced optical and electronic properties such as photochemical stability, tunable absorption and emission spectra, high molar absorption coefficient, high fluorescence quantum yields (QYs), and large Stokes shifts.[25,27–54] These enhanced photophysical properties of BN-substituted polycyclic compounds also make them ideal candidates for potential use in organic field-effect transistors (OFETs)[55–58] and organic light emitting diodes (OLEDs).[34,59–64] There is also an increasing demand for these functionalities in medicinal chemistry for biological molecular sensing/indicator applications.[24,65–67]

In spite of the fact that heterocyclic chemists have made significant strides in the development of BN-substituted polycyclic compounds,[68] a critical drawback of polycyclic aromatic systems partially substituted with a B–N bond, especially three-coordinate boron species, is that they tend to aggregate at high concentration or in the solid-state due to significant intermolecular π–π stacking interaction, which in turn results in emission quenching, *i.e.* aggregation-caused quenching (ACQ).[69–75] This photophysical phenomenon poses significant challenges when working with systems that require the operating fluorescent compound to display high QYs at high concentration or in the solid-state such as in the construction of OLEDs and chemical sensors. To remedy this ACQ problem, researchers have taken diverse approaches over the years and have recently adopted the concept of aggregation-induced emission (AIE) which was first introduced by Tang in 2001.[76] Since the introductory research on AIE by Tang, chemists have focused on developing new polycyclic aromatic chromophores with AIE features[77–82] but have given little attention to BN-substituted polycyclic aromatic compounds featuring AIE, especially three-coordinate boron species such as polycyclic aromatic 1,2-azaborines, and as result these species are still scarce in the literature.[83] In addition to the limited report of polycyclic aromatic 1,2-azaborines featuring AIE, only a handful of polycyclic 1,2-azaborine compounds have been reported to display minimal changes in their absorption wavelength and intensity of emission in solvents with different polarities, *i.e.* solvatochromism.[84,85] The study of BN-substituted polycyclic compounds such as 1,2-azaborines exhibiting solvatochromism are essential because they can be used as sensors for solvent polarity.[86,87]

Tang reported in 2022 the first and only example of a polycyclic 1,2-azaborine that exhibits both ACQ and AIE properties in a single BN-substituted polycyclic backbone.[69] Herein, we are reporting the first and only example of a polycyclic aromatic 1,2-azaborine that exhibits both AIE and solvatochromism properties in a single BN-substituted polycyclic backbone. This study will expand chemists' understanding in overcoming the ACQ problem in BN-substituted aromatic compounds, specifically three-coordinate boron, and will extend the scope of solvatochromic polycyclic 1,2-azaborines and the exploration of their new properties and functions. In this report, we describe the design and synthesis of three phenyl-substituted pyrrolidinone-fused 1,2-azaborines (PFAs) derivatives with similar structures and functionalized with diverse electronic moieties (–H, $–NO_2$, –CN, referred to as **PFA 1**, **2**, and **3**, respectively) containing a pre-twisted molecular structure (Fig. 1). Previously reported PFA analogs, **benzo-** and **nitrobenzo-azaborines**,[14,15] are also included in this study to highlight the impact of intramolecular rotations and steric interactions within the PFA framework on the observed photophysical properties. This new molecular design results in marked effects of solvatochromism and switchable fluorescence that can be completely "turned off" and "turned on"

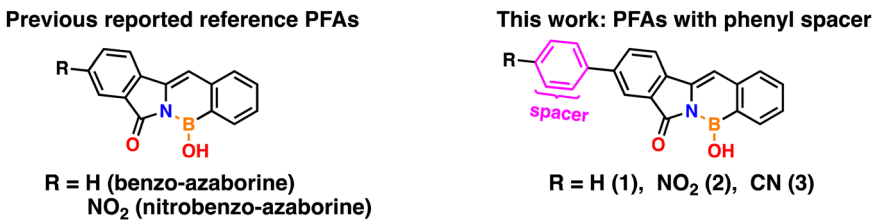

Fig. 1 The structures of PFA analogs and three new phenyl-substituted PFAs discussed in this work.

via AIE in **PFA 2**. Although **PFAs 1** and **3** show neither solvatochromism nor switchable fluorescence turn on and off *via* AIE, both are chemically stable with **PFA 1** in particular displays unexpectedly high QYs in the solid-state when compared to its analog, **benzo-azaborine**, and is worth further investigation as a promising candidate for OLED construction.[88–94]

Results and discussion

Syntheses and structural characterization

The synthesis of three new phenyl-substituted PFAs was conducted *via* a one-pot base-catalyzed condensation reaction of phenyl-substituted isoindolinone derivatives with the appropriate *o*-formylarylboronic acids. The PFAs were prepared using modified procedures developed by Huggins and coworkers.[14,15] The first phase of the synthetic scheme involves the synthesis of phenyl-substituted isoindolinones functionalized with diverse electronic moieties (–H, –NO_2, –CN) *via* carbon–carbon bond formation using a Suzuki cross-coupling transition-metal-catalyzed reaction (Scheme 1). The esterification of 5-bromo-2-methylbenzoic acid with methanol (MeOH) is performed to make compound **4** in high yields, followed by a Suzuki cross-coupling reaction with phenylboronic acid pinacol esters with corresponding electronic moiety substituents (–H, –NO_2, –CN) at the *para*-position to synthesize compounds **5–7** in good yields. Then, selective radical bromination of the aryl methyl group is carried out using *N*-bromosuccinimide (NBS) yielding both mono- and di-brominated isomers in nearly equal amount. The purified mono-brominated isomers **8–10** were then reacted with ammonia in MeOH to yield the phenyl-substituted isoindolinones **11–13** in high yields. The second phase of the synthetic scheme involves the synthesis of the new desired end-products, phenyl-substituted **PFAs 1–3**, which is conducted *via* a one-pot base-catalyzed condensation reaction of the conjugated phenyl-substituted isoindolinones with the appropriate *o*-formylarylboronic acids. The structures of previously unreported compounds **12**, **13** and **PFAs 1–3** were confirmed by ^{1}H, $^{13}C\{^{1}H\}$, $^{11}B\{^{1}H\}$ NMR spectroscopy, high-resolution mass spectrometry (HRMS) and FT-IR (see ESI†). $^{11}B\{^{1}H\}$ NMR spectrum for **PFAs 1**, **2** and **3** show a broad peak at 31.13, 30.39 and 29.64 ppm, respectively. The $^{11}B\{^{1}H\}$ resonance for **PFAs 1**, **2** and **3** corresponds to the boron atom bonded to a nitrogen atom and a hydroxyl group and are in line with previous reports of –N–B–OH π-bonding characteristics.[14,15] Additional assignments were based on 2D NMR experiments, and the spectra are presented in the ESI.† All compounds were stable under ambient conditions.

PFA 3 crystals of X-ray crystallography quality were obtained by the slow diffusion of petroleum ether (PE) into a saturated tetrahydrofuran (THF) solution at room temperature (21 °C). Fig. 2 depicts the molecular structure of **PFA 3** which displays a planar three-coordinate boron bonded to C, N, and O. The length of the B–N bond was measured to be 1.446 Å (Fig. 2A) and agrees with the sp^2 type B–N bond length previously reported for polycyclic 1,2-azaborine derivatives and borazine (1.44 Å).[14,95–97] An intramolecular hydrogen bond between the boron O–H and the C=O oxygen with a distance of 2.114 Å is also observed. Additionally, the molecular structure of **PFA 3** confirms the attachment of a phenyl spacer to the core

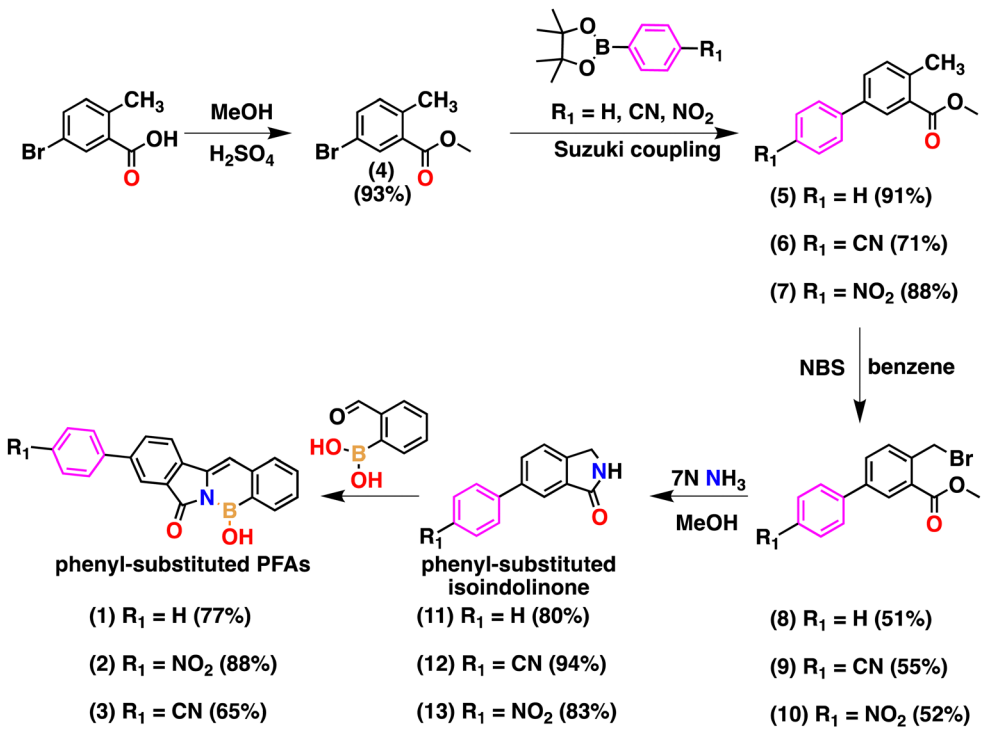

Scheme 1 Synthetic route to synthesize phenyl-substituted **PFAs 1–3**.

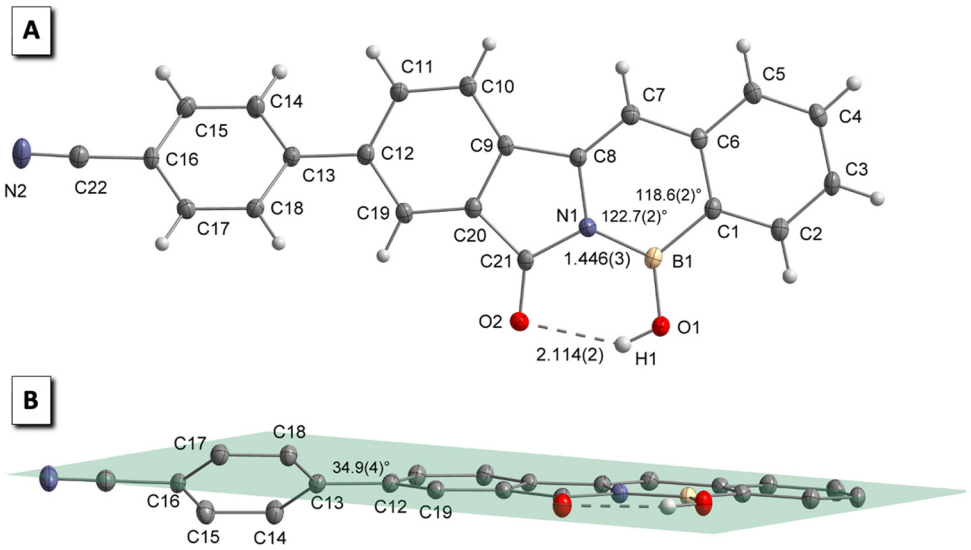

Fig. 2 (A) Molecular structure of **PFA 3** displaying the B–N bond length (1.466 Å) and the ring angles around the boron atom ∠C8N1B1 = 122.7° and ∠C6C1B1 = 118.6°. (B) Molecular structure of **PFA 3** displaying the planarity of the core (**benzo-azaborine**) and the rotation of the biphenyl moiety with a torsion angle of 34.9°. A single molecule is represented using ORTEP thermal ellipsoids drawn at 50% position probability (gray: carbon, red: oxygen; blue: nitrogen; white: hydrogen; yellow: boron).

(**benzo-azaborine**) *via* carbon–carbon bond formation and the presence of the –CN group. As projected, the molecular structure of **PFA 3** verifies the planarity of the core (**benzo-azaborine**) and shows rotation around the carbon–carbon bond of the biphenyl moiety with a torsion angle of 34.9° (Fig. 2B).

Experimental photophysical properties

Absorption spectra

The relevant absorption properties for **PFAs 1–3**, along with analogs compounds, **benzo-** and **nitrobenzo-azaborines**, were investigated in various solvents with different polarities and hydrogen-bonding abilities to examine the impact of intramolecular rotations and steric interactions within the PFA framework on the observed photophysical properties (Table 1). **PFAs 1–3** show strong absorption bands lying in the region of 380–385 nm in all solvents except for **PFAs 2** and **3** in dimethyl sulfoxide (DMSO). In DMSO, **PFAs 2** and **3** show strong absorption bands in the region of 390 nm and 400 nm, respectively. Additionally, to fully comprehend the effect of the phenyl spacer on the optical properties of the PFAs, the frontier molecular orbitals (HOMO and LUMO) for **1–3** along with reference compounds, **benzo-** and **nitrobenzo-azaborines** and their energies involved in the electronic transition were studied theoretically by density functional theory (DFT) calculations at the level of B3LYP/6-311+G** (Fig. 3). This level of theory was used to compare to past reported results that were calculated at the same level. The addition of a phenyl linker to **benzo-azaborine**, as for **PFA 1**, extends its π-conjugation, resulting in a red-shifted absorbance λ_{max} in all solvents by an average of 10 nm. The DFT analysis from Fig. 3 illustrates that increased π-conjugation of **PFA 1** results in a reduction of the HOMO–LUMO gap by 0.10 eV, rationalizing the red-shift in absorbance seen for **PFA 1** when compared to

Table 1 Experimental UV-visible absorbance (λ_{max}), molar absorption coefficient (ε), and solid-state excitation (λ_{max}) data for **PFAs 1–3** with reference compounds, **benzo-** and **nitrobenzo-azaborines** in various solvents

Cmpds	Solvents	λ_{max} (nm) in solution	(ε)	λ_{max} (nm) solid-state
Benzo-azaborine	$CHCl_3$	375	(1.8×10^4)	389, 416
	CH_3OH	372	(3.2×10^4)	
	CH_3CN	371	(2.0×10^4)	
	DMSO	372	(2.9×10^4)	
	THF	370	(1.4×10^4)	
Nitrobenzo-azaborine	$CHCl_3$	388	(3.7×10^4)	397, 424
	CH_3OH	412	(1.2×10^4)	
	CH_3CN	382	(1.8×10^4)	
	DMSO	404	(2.4×10^4)	
	THF	385	(1.2×10^4)	
1	$CHCl_3$	385	(1.4×10^4)	392, 414
	CH_3OH	380	(1.3×10^4)	
	CH_3CN	380	(1.7×10^4)	
	DMSO	385	(2.4×10^4)	
	THF	380	(1.8×10^4)	
2	$CHCl_3$	385	(1.1×10^4)	394, 420
	CH_3OH	[a]	[a]	
	CH_3CN	380	(3.7×10^3)	
	DMSO	400	(9.6×10^3)	
	THF	380	(2.6×10^4)	
3	$CHCl_3$	385	(1.8×10^4)	392, 416
	CH_3OH	[a]	[a]	
	CH_3CN	[a]	[a]	
	DMSO	390	(2.3×10^4)	
	THF	380	(1.7×10^4)	

[a] Absorption and molar absorption coefficient could not be obtained due to low solubility in solvent.

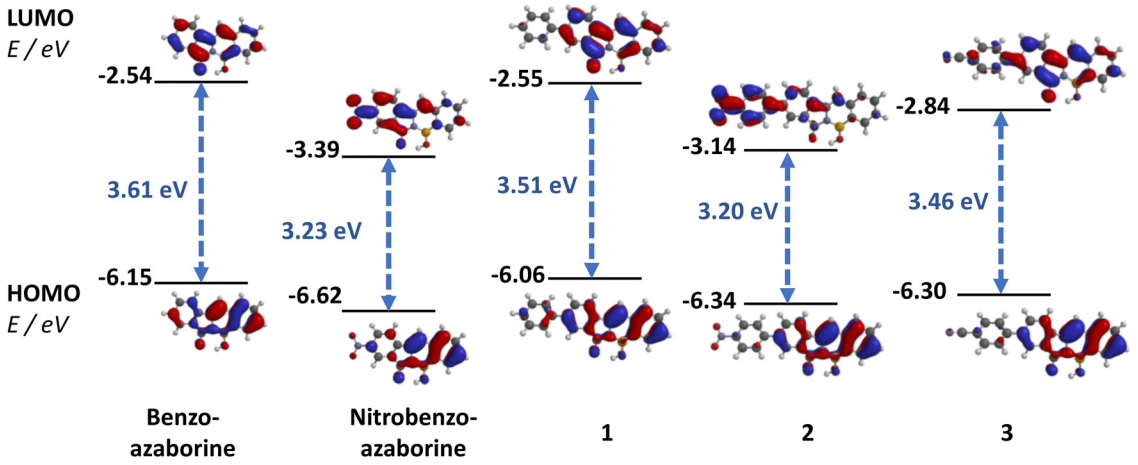

Fig. 3 Frontier molecular orbitals (HOMO and LUMO), computed using B3LYP/6-311+G**, for **PFAs 1–3** along with reference compounds, **benzo-** and **nitrobenzo-azaborines** and their corresponding electronic transition energies.

benzo-azaborine. Surprisingly, the addition of a phenyl spacer to **nitrobenzo-azaborine**, as for **PFA 2**, does not result in a similar red-shift in absorbance. Instead, **PFA 2** has a similar absorbance to its analog **nitrobenzo-azaborine**, and DFT analysis shows a very similar HOMO–LUMO profile (Fig. 3). We also observe similar absorbance λ_{max} for **PFAs 1** and **2** in all solvents except for DMSO, in which **2** exhibits a 15 nm red-shift in the absorbance λ_{max}. Based on the generally similar absorbances of **PFA 2** to **PFA 1**, it is evident that incorporation of the phenyl spacer to **nitrobenzo-azaborine** reduces the influence of the electron-accepting nature of the $-NO_2$ group on the PFA core. To further understand the effect of the phenyl spacer on the electronic changes induced by electron-accepting substituents, the –CN group of **PFA 3** was chosen for its comparable Hammett Sigma *para* value (σ_p = 0.66) to $-NO_2$ (σ_p = 0.78).[98] The absorbance λ_{max} of **PFAs 2** and **3** were identical in chloroform ($CHCl_3$) and THF. However, DMSO induces a 10 nm blue-shifted absorbance accompanied by an increase in molar absorptivity for **PFA 3**. The absorbances and molar absorptivities for **3** also mirrored that of **1** in all solvents. The addition of the –CN group to **PFA 1** reduces the energy of both HOMO and LUMO almost proportionately, resulting in an almost identical HOMO–LUMO gap for **PFA 3** and **PFA 1**. Additionally, **PFA 3** has a similar HOMO and LUMO electron density distribution to that of **PFA 1**, with electron density distributed primarily throughout the PFA core and minimal electron density on the phenyl spacer bearing the –CN group. Based on the comparable absorbances seen for **PFAs 2** and **3**, and their similar absorbances to **PFA 1**, we conclude that the addition of a phenyl spacer on Acceptor–π–Donor (A–π–D) PFAs results in a decoupling of the $-NO_2$ and –CN groups from the PFA core due to the intramolecular rotation around the biphenyl moiety.

The solid-state excitations of the PFAs were also measured by drop-casting concentrated solutions of $CHCl_3$ (Table 1). Due to aggregation in the solid-state, dual excitations are observed for all PFAs. Furthermore, all PFAs display red-shifted solid-state excitation λ_{max} in comparison to being in solution due to solid-state π–π stacking interactions. **PFAs 1**, **3** and **benzo-azaborines** have almost identical solid-state excitation while the nitro-substituted PFAs, **PFA 2** and **nitrobenzo-azaborine**, exhibit the most red-shifted solid-state excitation. These results demonstrate a solution trend in which extending π-conjugation *via* incorporation of a phenyl linker reduces the HOMO–LUMO gap and results in red-shifted absorbance λ_{max}. We also observe a solid-state trend in which incorporation of a phenyl spacer on A–π–D PFAs results in blue-shifted absorbance λ_{max} due to a decoupling of the electron-accepting $-NO_2$ and –CN groups from the PFA core.

Emission spectra

The relevant emission properties for **PFAs 1–3** along with reference compounds, **benzo-** and **nitrobenzo-azaborines**, were studied in various solvents with different polarities and hydrogen-bonding abilities and are displayed in Table 2. The emission spectrum of **PFA 2** in MeCN displays intriguing features with a very weak emission accompanied by two λ_{max} at 447 nm and 656 nm. The QYs were very low and could not be quantified, as evidenced by the absence of visible emission from the vial containing **2** in MeCN (Fig. 4A). The more intense emission λ_{max} appears at 447 nm with a Stokes shift of 3945 cm^{-1} and the weak, red-shifted emission λ_{max} shows up at 656 nm with a Stokes shift of 11 072 cm^{-1}. The 447 nm emission λ_{max} is similar to that of **PFAs 1** and **3**, which suggests that this emission occurs from a state common to all three PFAs. The weak, red-shifted emission λ_{max} at 656 nm is expected to be due to an ICT state with complete charge separation within **PFA 2** as depicted in the computed frontier molecular orbitals in Fig. 3. Such a twisted charge-separated state is expected to be stabilized by higher polarity solvents such as MeCN, consistent with the broad, red-shifted spectrum with its emission λ_{max} at 656 nm (Fig. 4A). Such an ICT state is unique to **PFA 2** in MeCN and results in a significant quenched fluorescence at λ_{max} 447 nm, whereas the fluorescence of

Table 2 Fluorescence data for **PFAs 1–3** with reference compounds, **benzo-azaborine** and **nitrobenzo-azaborine** in various solvents and in the solid-state

Cmpds	Solvents	λ_{em} (nm)	(Φ_F) in solution	Stokes Shift (nm)	Stokes Shift (cm^{-1})	λ_{em} (nm) (Φ_F) solid-state
Benzo-azaborine	$CHCl_3$	437	0.97	62	3783	465 (0.09)
	CH_3OH	430	0.94	58	3625	
	CH_3CN	432	1.00	61	3806	
	DMSO	438	1.00	66	4050	
	THF	434	1.00	64	3986	
Nitrobenzo-azaborine	$CHCl_3$	521	0.06	133	6580	493 (0.005)
	CH_3OH	[b]	[b]	n/a	n/a	
	CH_3CN	563	0.002	181	8416	
	DMSO	[b]	[b]	[b]	[b]	
	THF	523	0.04	138	6853	
1	$CHCl_3$	443	0.77	58	3400	513 (0.32)
	CH_3OH	436	0.73	56	3380	
	CH_3CN	443	0.62	63	3742	
	DMSO	449	0.81	64	3702	
	THF	442	0.87	62	3691	
2	$CHCl_3$	[a]	[a]	[a]	[a]	476, 540 (0.01)
	CH_3OH	[a]	[a]	[a]	[a]	
	CH_3CN	447, 656	[c]	67, 276	3945, 11072	
	DMSO	[b]	[b]	[b]	[b]	
	THF	524	0.01	144	7230	
3	$CHCl_3$	447	0.50	62	3600	465 (0.13)
	CH_3OH	470	0.94	n/a	n/a	
	CH_3CN	443	0.24	n/a	n/a	
	DMSO	450	1.00	60	3418	
	THF	442	1.00	62	3690	

[a] Fluorescence could not be obtained due to low solubility. [b] Fluorescence was not observed in selected solvents. [c] Quantum yields could not be obtained in selected solvents or in the solid-state.

PFAs 1 and **3** is persistently visible. Despite also containing an electron-accepting group, the features of the emission spectra of **PFA 3** show surprisingly similar emission λ_{max} and Stokes shift to **PFA 1** in all solvents except from MeOH (Table 2). This result suggests that the ICT state accessible for **PFA 2** is energetically inaccessible in **PFA 3**. An increase in QYs is also observed for **PFA 3** in MeCN in comparison to **PFA 2** and the weak, red-shifted emission peak at 656 nm is absent (Fig. 4A), both of which indicate that the presence of the $-NO_2$ group is essential to produce the ICT process seen in **PFA 2**.

It is important to interpret the results in Fig. 3 with caution, since the B3LYP functional notoriously overstabilizes charge transfer excitation energies, yielding artificially lower LUMOs.[99] Therefore, we carried out DFT and time-dependent DFT (TD-DFT) calculations using the CAM-B3LYP functional and 6-31+G* basis set.[100] The CAM-B3LYP functional includes a long-range correction that removes the self-interaction error of B3LYP. The CAM-B3LYP optimized ground-state structures of **PFAs 1–3** closely resemble each other, displaying the same degree of twisting of the terminal, substituted phenyl ring (Fig. 6). In all three molecules, the torsional deformation of that ring is *ca.* 37° which is in good agreement with the biphenyl torsional angle measurement (35°) from the X-ray crystal structure of **PFA 3**. The TD-DFT calculations immediately reveal important differences in **PFA 2** compared to **PFAs 1** and **3**. The natural transition orbitals (NTOs) reveal that **PFAs 1** and **3** possess one excited state which is the locally excited state (S_1). Whereas, **PFA 2** has the same locally excited state (S_1) as that observed in **1** and **3** and an additional, second excited state (S_2) due to a prominent n–π* transition centered on the nitrophenyl substituent (Fig. 5).

As shown from the photophysical property sections, the optical properties of the PFA core (**benzo-azaborine**) and **PFA 1** are independent of solvent polarity or hydrogen-bonding ability and show no solvatochromism. Therefore, any observed photophysical changes based on solvent effects should be directly attributed to a charge transfer state, which is much more sensitive to the solvent polarity due to its charge-separated character. The fluorescence properties for **PFAs 1–3** were measured in THF, which is less polar than MeCN, to study their fluorescence solvatochromism and to determine whether the ICT process seen in **PFA 2** is responsible for the fluorescence quenching in MeCN. Interestingly, we observed solvatochromism for **PFA 2** in THF as a broad red-shift in emission λ_{max} (from 447 nm to 524 nm) (Fig. 4B), an increase in QYs, and a large Stokes shift of 7,230 cm^{-1} (Table 2); however, no significant changes were observed for **PFAs 1** and **3** in THF.

While it may be tempting to assign this broad emission in THF to less solvent-stabilized ICT state, the computations in Fig. 6 suggest the presence of a n–π* transition on the nitrophenyl substituent may be important for the solvent-dependent absorbance and fluorescence properties of **PFA 2**. To observe if

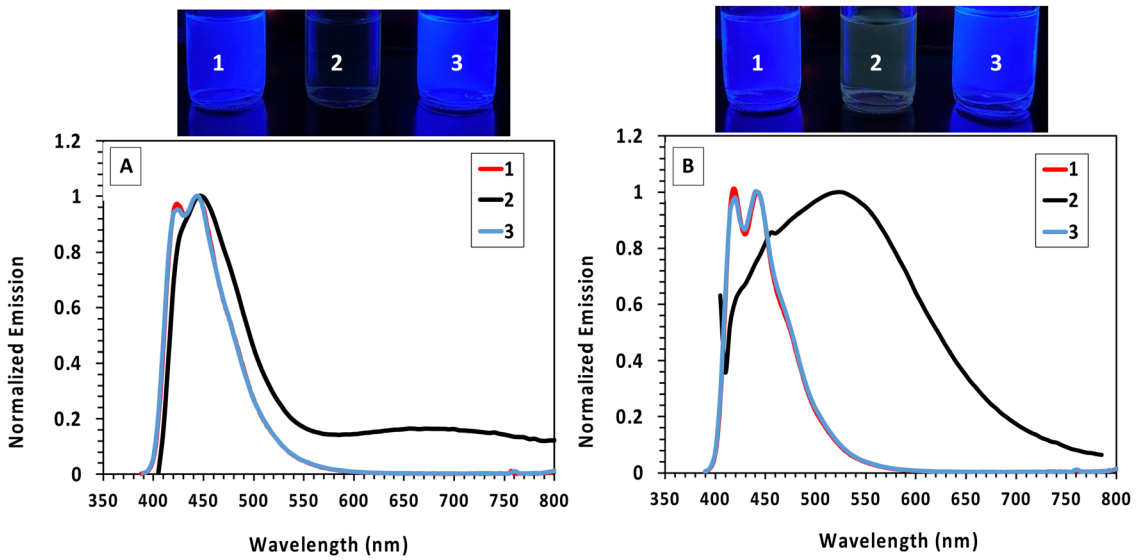

Fig. 4 Emission spectra of **PFAs 1–3** in MeCN (A) and THF (B). Solutions were excited at their respective absorption maxima. The top panel illustrates pictures of **PFAs 1–3** in MeCN (left) and in THF (right) under a 365 nm handheld UV-light lamp. Data points for **1** and **3** are essentially overlaid.

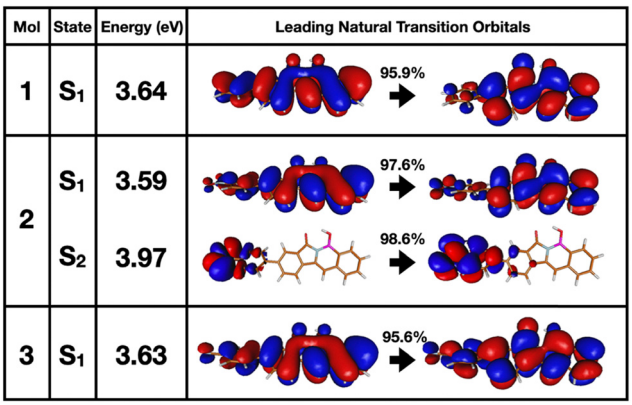

Fig. 5 The NTO pairs with the highest weight in describing the S_1 excitations in **PFAs 1**, **2**, and **3**. The S_2 excitation is also shown for **PFA 2**.

such n–π* transition is energetically accessible, we optimized the excited-state structures of **PFAs 1-3** using TD-DFT and accounted for the solvent using a polarizable continuum model (PCM) to account for the dielectric environment of THF. The choice of THF in the calculation is to explain the unusual, broad experimental emission band appearing at λ_{max} of 524 nm. We found that upon optimizing the excited state structure of **PFA 2**, the n–π* excited state (orange in Fig. 6) decreases in energy and becomes lower in energy than the π–π* excited-state (black). The vertical emission energy computed at the TD-DFT level of theory with CAM-B3LYP/6-31+G* with a THF solvent model is 2.33 eV (526 nm), in very good agreement with the experimental emission wavelength observed in THF (524 nm). Therefore, we conclude that the fluorescence observed in THF is likely due to the presence of a unique n–π* state in **PFA 2** that does not exist in **PFA 1** and **PFA 3**. To check the results of the CAM-B3LYP calculations, we performed the same calculations at the wB97X-D level of theory[101] and obtained quantitatively similar results (with state energies within 0.1 eV of the CAM-B3LYP results). This result suggests that the relative energies of **PFA 2** strongly depend on the solvent polarity, causing strong solvatochromism, with emission being tunable by adjusting solvent polarity from MeCN to THF. It also indicates that the ICT state from **PFA 2** in MeCN is responsible for the quenched fluorescence since the fluorescence is recovered in THF with no ICT band.

We were also interested to learn how the formation of aggregates will affect the fluorescence and ICT process of **PFA 2** since its fluorescence is quenched in MeCN. We hypothesized that formation of aggregates by increasing fractions of water (f_w) in MeCN solution will generate π–π stacking interaction among **PFA 2** molecules, thus enhancing emission intensity, and red-shifting the fluorescence *via* J-aggregation. The fluorescence spectra of **PFA 2** were measured in an MeCN/water mixture with varying volume fractions of water f_w = 0 to 0.95 at 0.10 increments. When water is added, the emission at 656 nm, attributed to the ICT process, is weakened, and disappears at f_w = 30 (Fig. 7B). The emission λ_{max} at 447 nm starts to increase at f_w = 60 due to formation of the aggregates and continues to intensify (Fig. 7B) and red-shifts with increasing f_w. The formation of aggregates at f_w = 0.60 is coincident with enhancement of the emission; therefore, **PFA 2** is confirmed to exhibit aggregation-induced emission (AIE). The photograph in Fig. 7A shows a green fluorescence is recovered upon the formation of aggregates. The red-shifting of emission from the aggregate sample (with monomer emission from ICT process disappearing and from the locally excited state moving from λ_{em} 447 nm to λ_{em} 470 nm), is a clear signature of J-aggregation facilitating delocalization of the excited energy over multiple **PFA 2** chromophores. The tendency for the fluorescence to be recovered by the formation of **PFA 2** aggregates

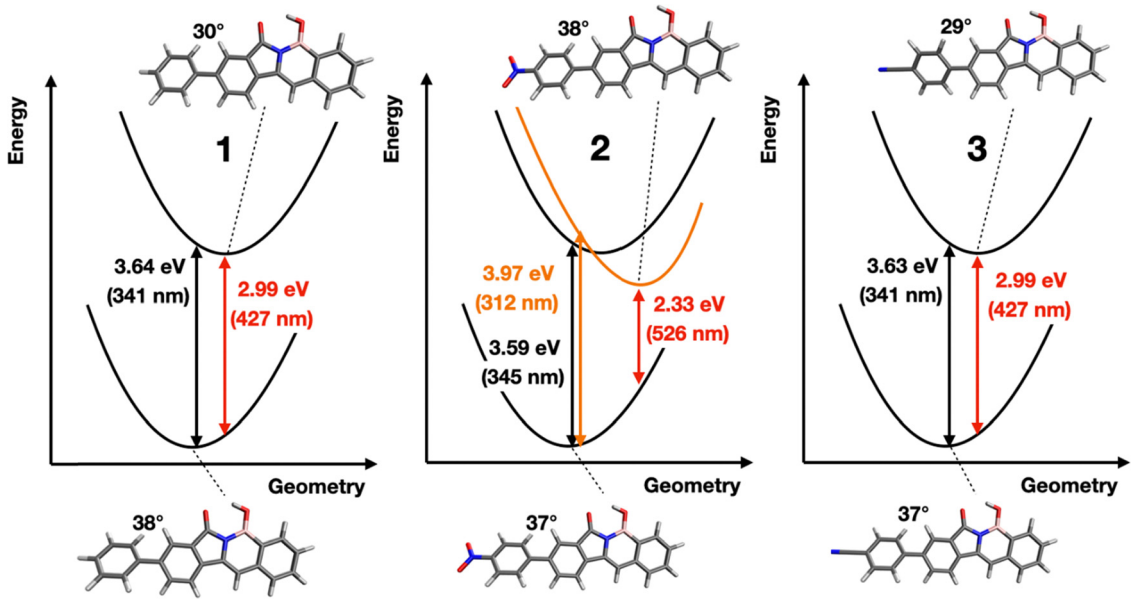

Fig. 6 A diagram representing electronic states of **PFAs 1**, **2**, and **3** schematically as harmonic potentials. The lower potential represents the ground state (S_0). The black potentials above indicate the locally excited state, which corresponds to the S_1 state for molecules **1**, **2**, and **3**. The orange potential represents the n–π* S_2 state of molecule **2**. While the locally excited states have more planar excited state geometries for **PFAs 1** and **3**, the n–π* transition of **PFA 2** results in an excited state that remains twisted or becomes slightly more twisted relative to the ground state. The vertical excitation and emission energies are indicated in eV and in nm for each molecule. The optimized lowest energy S_0 and S_1 states are shown below and above the energy diagram, respectively, with the torsional angle of the biphenyl moiety labeled.

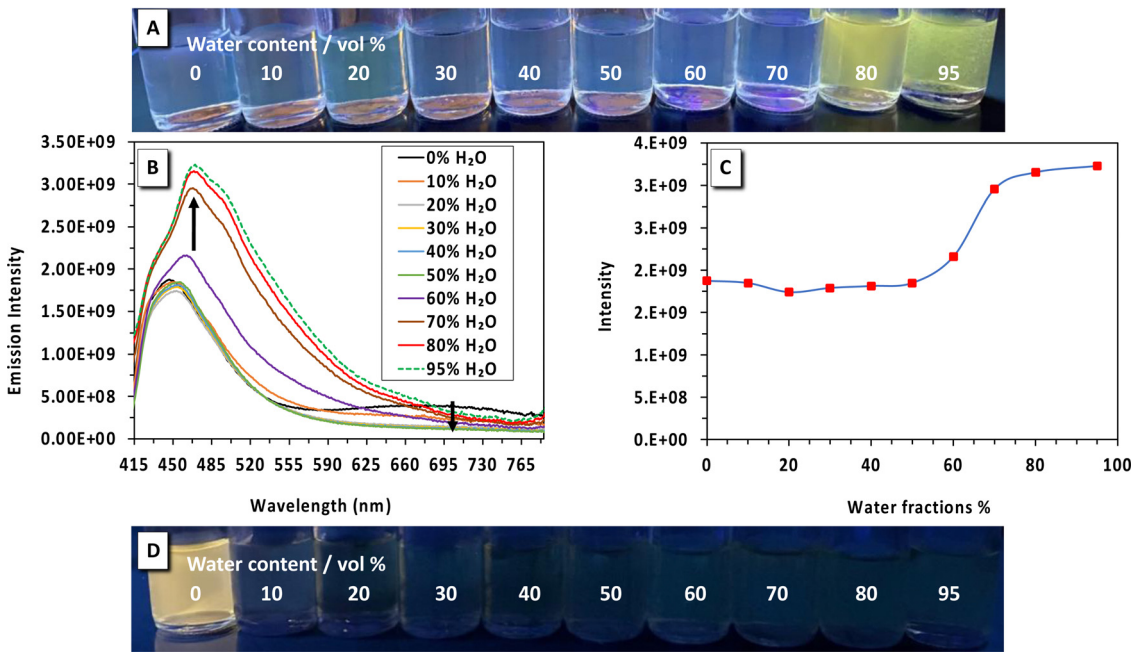

Fig. 7 The top panel (A) illustrates a picture of **PFA 2** in MeCN (concentration = 10^{-4} M) with increasing fractions of water under a 365 nm handheld UV-light lamp. (B) Emission spectra of **PFA 2** in MeCN/water mixtures (0–95% water). (C) Plot of fluorescence intensity of **PFA 2** *vs.* % of water fraction (f_w). (D) Picture of **nitrobenzo-azaborine** in MeCN (concentration = 10^{-4} M) upon increasing the fraction of water under a 365 nm handheld UV-light lamp.

suggests that aggregation stabilizes the locally excited π–π* state, making access to the n–π* state less energetically favorable. **PFAs 1** and **3** were also examined for AIE and J-aggregation in MeCN/water by the same methods, but no evidence of AIE or J-aggregation for **PFAs 1** and **3** was observed (see ESI†).

We also investigated the effect of the phenyl spacer on the AIE seen in **PFA 2**. We conducted identical experiments in MeCN/water solution for **nitrobenzo-azaborine** (analog with no phenyl spacer). Unexpectedly, the opposite effect was observed for **nitrobenzo-azaborine** when compared to **PFA 2**. The

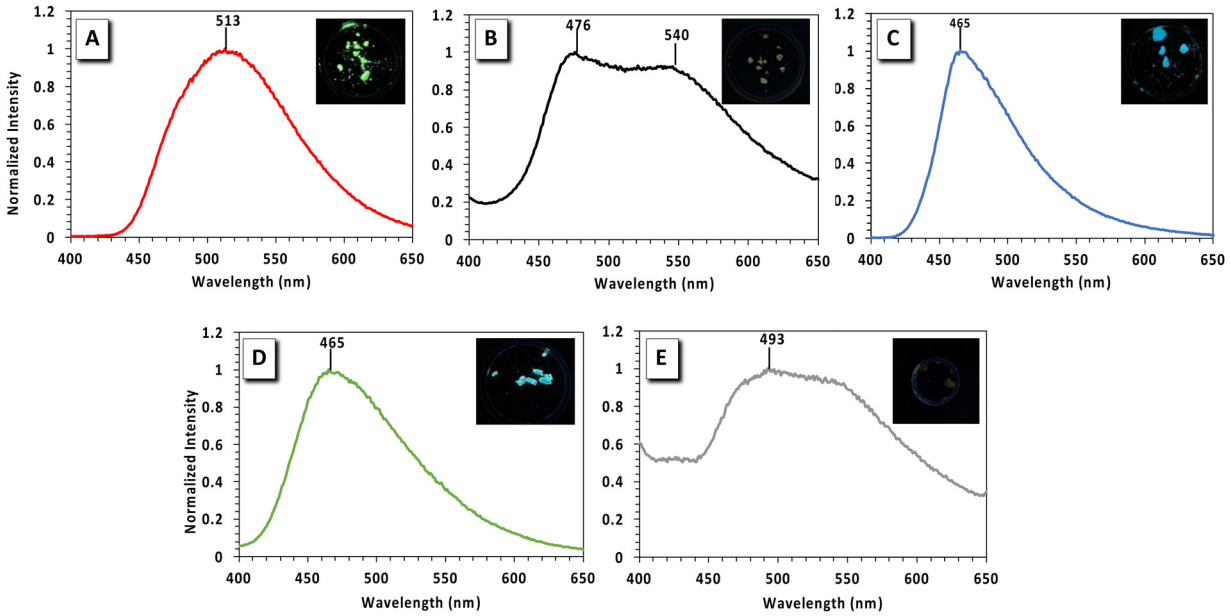

Fig. 8 Solid-state emission spectra of **PFAs 1–3** and reference compounds, **benzo-** and **nitrobenzo-azaborines**, as (A)–(C) and (D)–(E), respectively.

addition of water fractions to an MeCN solution of **nitrobenzo-azaborine** immediately quenches the ICT emission due to aggregation-caused quenching (ACQ) as displayed from the photograph in Fig. 7D. This observation suggests that the addition of a phenyl spacer to A–π–D nitro-substituted polycyclic aromatic 1,2-azaborine, **nitrobenzo-azaborine**, creating a pre-twisted molecular structure is necessary to generate AIE instead of ACQ. This result reinforces our hypothesis that the formation of aggregates quenches the ICT state and stabilizes the locally excited π–π* state for **PFA 2**.

The solid-state emission spectra of the PFAs were also investigated to get better insight into their intermolecular interactions (Fig. 8). Due to π–π stacking interactions in the solid-state, the emission wavelengths of the PFAs were red-shifted when compared to being in solution (Table 2), except for **nitrobenzo-azaborine** and **PFA 2** in MeCN due to the ICT process in solution. On average, the solid-state emission λ_{max} for **benzo-azaborine** is red-shifted by 30 nm (435 nm to 465 nm) in comparison to the emission λ_{max} in solution. The addition of a phenyl linker to **benzo-azaborine** which extends π-conjugation, as for **PFA 1**, results in higher QYs (from 0.09 to 0.32) and red-shifts the solid-state emission λ_{max} by 48 nm when compared to **benzo-azaborine**. Importantly, an increase in solid-state QYs is a valuable feature for OLED development.[88–94] **PFA 2** also exhibits a 70 nm red shift in solid-state emission λ_{max} *versus* solution. Both **nitrobenzo-azaborine** and **PFA 2** display significantly lower QYs than the other compounds due to intersystem crossing where addition of a $-NO_2$ group to a fluorophore is known to decrease fluorescence.[102] The emission λ_{max} at 476 nm for **PFA 2** in the solid-state can be attributed to a state that is localized on the PFA core and is common to all three PFAs. Conversely, the red-shifted emission λ_{max} at 540 nm is due to distinct state that is unique to the $-NO_2$ substitution. Varying the $-NO_2$ group of **2** with a –CN group of **3** allows for analysis of the electronic effect of different electron-accepting moieties in the solid-state. On average, the solid-state emission λ_{max} for **PFA 3** is red-shifted by 15 nm (450 nm to 465 nm) in comparison to solution emissions. Unexpectedly, the solid-state emission of **PFA 3** is identical to that of **benzo-azaborine** (no phenyl spacer) with similar QYs, regardless of the presence of an electron-accepting group. This result indicates that having dual emission wavelengths is unique to the compounds containing an $-NO_2$ group since dual emission for **PFA 3** was not observed, and only the core-localized excited state process was observed in the emission spectrum, consistent with the **benzo-azaborine** observations.

Conclusions

In conclusion, we report the synthesis, characterization, experimental and computational analysis of three phenyl-substituted PFAs with similar structures and functionalized with diverse electronic moieties (–H, $-NO_2$, –CN, referred to as **PFA 1**, **2**, and **3**, respectively) containing a pre-twisted molecular structure. This new molecular design results in fluorescence that can be completely ''turned off'' and ''turned on'' *via* aggregation-induced emission (AIE) in **PFA 2** and solvatochromism. The absorption and emission of both **PFAs 1** and **3** can largely be explained by a single π–π* state due to excitation largely localized on the PFA core. However, the photophysics of **PFA 2** are complicated by the presence of the $-NO_2$ group; in addition to a locally excited π–π* state on the PFA core, the spectral features of **PFA 2** also indicate the presence of a low-lying n–π* state centered on the $-NO_2$ group and ICT states that can red-shift and quench fluorescence. The relative energies of those states strongly depend on the solvent polarity, causing

strong solvatochromism in **PFA 2**, with emission being tunable by adjusting solvent polarity from MeCN to THF. We hypothesize that the more polar MeCN stabilizes an ICT state with strongly red-shifted and weak fluorescence. However, the ICT is inaccessible in the less polar THF, such that the photophysics in THF are instead dominated by a low-lying n–π* state that fluoresces at around 524 nm. Increasing the volume fractions of poor solvents such as water into dilute MeCN solution of **PFA 2** induces aggregation. The formation of aggregates in f_w 0.60 coincides with enhancement of the emission through aggregation-induced emission (AIE). Aggregation stabilizes the locally excited PFA core π–π* state through J-aggregation relative to the n–π* state and quenched ICT states, thereby increasing the overall fluorescence intensity. Although **PFAs 1** and **3** show neither solvatochromism nor switchable fluorescence *via* AIE, both are chemically stable, with **PFA 1** displaying unexpectedly high QYs in the solid-state when compared to reference, **benzo-azaborine**, and should be further investigated as a promising candidate for the construction of OLEDs.

Data availability

All the data have been included in the ESI.†

Author contributions

Conceptualization and supervision – C. J. S. L.; methodology – A. D. C., K. E., L. K. G., J. E. R., R. B. H., A. M. B., P. D. B., R. M.; formal analysis – A. D. C., K. E., L. K. G., O. A. S. (collected absorbance and emission data); formal analysis – K. K. H., V. V. L., R. J. G. (collected excitation and QYs data); formal analysis – C. J. S. L., S. O. A, and S. G. (computational resources); formal analysis – C. J. S. L., and L. W. (crystallography); writing – original draft, C. J. S. L.; writing – review & editing, C. J. S. L., A. D. C., O. A. S., R. J. G, S. O. A, and S. G.

Conflicts of interest

The authors declare no competing financial interest.

Acknowledgements

We thank the Peach State Bridges to the Doctorate Program from Kennesaw State University (KSU) for fellowship support for A. D. C. (NIH-1T32GM150548-01), and the Peach State Louis Stokes Alliance for Minority Participation (LSAMP) from KSU for support for R. M. (NSF-2207368). We also thank Mentor Protégé Research Program from KSU for research funding. S. G. acknowledges National Science Foundation (NSF) XSEDE for computational resources through Research Allocation (CHE-180027). S. O. A. acknowledges NSF for fellowship support (CHE-2047667). R. J. G. acknowledges the NSF Chemical Synthesis Program (CHE-2046544) for a Hamamatsu C11347-11 Quantaurus-QY Absolute PL Quantum Yield Spectrometer used for optical spectroscopic analyses. We thank NSF CHE MRI 1828078 and UA for the purchase of the single crystal X-Ray diffraction instrument. The authors would like to thank Dr. Jimmy (Zhenming) Du for his assistance with the 2D NMR experiments.

References

1 M. D. Watson, A. Fechtenkötter and K. Müllen, *Chem. Rev.*, 2001, **101**, 1267–1300.
2 L. Schmidt-Mende, A. Fechtenkötter, K. Müllen, E. Moons, R. H. Friend and J. D. MacKenzie, *Science*, 2001, **293**, 1119–1122.
3 J. Wu, W. Pisula and K. Müllen, *Chem. Rev.*, 2007, **107**, 718–747.
4 D. Ding, J. Liang, H. Shi, R. T. K. Kwok, M. Gao, G. Feng, Y. Yuan, B. Z. Tang and B. Liu, *J. Mater. Chem. B*, 2014, **2**, 231–238.
5 M. Klikar, P. Solanke, J. Tydlitát and F. Bureš, *Chem. Rec.*, 2016, **16**, 1886–1905.
6 W. Aigner, O. Bienek, B. P. Falcão, S. U. Ahmed, H. Wiggers, M. Stutzmann and R. N. Pereira, *Nanoscale*, 2018, **10**, 8042–8057.
7 S. Jhulki and J. N. Moorthy, *J. Mater. Chem. C*, 2018, **6**, 8280–8325.
8 M. Stępień, E. Gońka, M. Żyła and N. Sprutta, *Chem. Rev.*, 2017, **117**, 3479–3716.
9 Q. Miao, *Adv. Mater.*, 2014, **26**, 5541–5549.
10 X.-Y. Wang, X. Yao, A. Narita and K. Müllen, *Acc. Chem. Res.*, 2019, **52**, 2491–2505.
11 K. Dhbaibi, L. Favereau and J. Crassous, *Chem. Rev.*, 2019, **119**, 8846–8953.
12 M. Hirai, N. Tanaka, M. Sakai and S. Yamaguchi, *Chem. Rev.*, 2019, **119**, 8291–8331.
13 M. J. S. Dewar, V. P. Kubba and R. Pettit, *J. Chem. Soc.*, 1958, 3073–3076.
14 C. J. Saint-Louis, L. L. Magill, J. A. Wilson, A. R. Schroeder, S. E. Harrell, N. S. Jackson, J. A. Trindell, S. Kim, A. R. Fisch, L. Munro, V. J. Catalano, C. E. Webster, P. P. Vaughan, K. S. Molek, A. K. Schrock and M. T. Huggins, *J. Org. Chem.*, 2016, **81**, 10955–10963.
15 C. J. Saint-Louis, R. N. Shavnore, C. D. C. McClinton, J. A. Wilson, L. L. Magill, B. M. Brown, R. W. Lamb, C. E. Webster, A. K. Schrock and M. T. Huggins, *Org. Biomol. Chem.*, 2017, **15**, 10172–10183.
16 Z. Liu and T. B. Marder, *Angew. Chem., Int. Ed.*, 2008, **47**, 242–244.
17 K. K. Hollister, A. Molino, G. Breiner, J. E. Walley, K. E. Wentz, A. M. Conley, D. A. Dickie, D. J. D. Wilson and R. J. Gilliard, *J. Am. Chem. Soc.*, 2022, **144**, 590–598.
18 K. K. Hollister, W. Yang, R. Mondol, K. E. Wentz, A. Molino, A. Kaur, D. A. Dickie, G. Frenking, S. Pan, D. J. D. Wilson and R. J. Gilliard Jr., *Angew. Chem., Int. Ed.*, 2022, **61**, e202202516.
19 K. E. Wentz, A. Molino, L. A. Freeman, D. A. Dickie, D. J. D. Wilson and R. J. Gilliard, *J. Am. Chem. Soc.*, 2022, **144**, 16276–16281.

20 K. E. Wentz, A. Molino, L. A. Freeman, D. A. Dickie, D. J. D. Wilson and R. J. Gilliard, *Inorg. Chem.*, 2021, **60**, 13941–13949.
21 C. Xu, A. Wakamiya and S. Yamaguchi, *J. Am. Chem. Soc.*, 2005, **127**, 1638–1639.
22 S. Saito, K. Matsuo and S. Yamaguchi, *J. Am. Chem. Soc.*, 2012, **134**, 9130–9133.
23 J. Huang and Y. Li, *Front. Chem.*, 2018, **6**, 341.
24 P. Zhao, D. O. Nettleton, R. G. Karki, F. J. Zécri and S.-Y. Liu, *ChemMedChem*, 2017, **12**, 358–361.
25 S. Wang, D.-T. Yang, J. Lu, H. Shimogawa, S. Gong, X. Wang, S. K. Mellerup, A. Wakamiya, Y.-L. Chang, C. Yang and Z.-H. Lu, *Angew. Chem., Int. Ed.*, 2015, **54**, 15074–15078.
26 Y.-H. He, F.-M. Xie, H.-Z. Li, K. Zhang, Y. Shen, F. Ding, C.-Y. Wang, Y.-Q. Li and J.-X. Tang, *Mater. Chem. Front.*, 2023, **7**, 2454–2463.
27 J.-Y. Wang and J. Pei, *Chinese Chem. Lett.*, 2016, **27**, 1139–1146.
28 I. S. Park, M. Numata, C. Adachi and T. Yasuda, *Bull. Chem. Soc. Jpn.*, 2015, **89**, 375–377.
29 Y. Zhang, D. Zhang, J. Wei, Z. Liu, Y. Lu and L. Duan, *Angew. Chem., Int. Ed.*, 2019, **58**, 16912–16917.
30 S. Nakatsuka, N. Yasuda and T. Hatakeyama, *J. Am. Chem. Soc.*, 2018, **140**, 13562–13565.
31 X.-Y. Wang, F.-D. Zhuang, J.-Y. Wang and J. Pei, *Chem. Commun.*, 2015, **51**, 17532–17535.
32 S. Hashimoto, T. Ikuta, K. Shiren, S. Nakatsuka, J. Ni, M. Nakamura and T. Hatakeyama, *Chem. Mater.*, 2014, **26**, 6265–6271.
33 W. Zhang, F. Zhang, R. Tang, Y. Fu, X. Wang, X. Zhuang, G. He and X. Feng, *Org. Lett.*, 2016, **18**, 3618–3621.
34 G. Li, Y. Zhao, J. Li, J. Cao, J. Zhu, X. W. Sun and Q. Zhang, *J. Org. Chem.*, 2015, **80**, 196–203.
35 X. Wang, F. Zhang, J. Liu, R. Tang, Y. Fu, D. Wu, Q. Xu, X. Zhuang, G. He and X. Feng, *Org. Lett.*, 2013, **15**, 5714–5717.
36 X. Yang, P. Zhao, J. Qu and R. Liu, *Luminescence*, 2015, **30**, 592–599.
37 J. F. Martínez Hardigree and H. E. Katz, *Acc. Chem. Res.*, 2014, **47**, 1369–1377.
38 X.-Y. Wang, H.-R. Lin, T. Lei, D.-C. Yang, F.-D. Zhuang, J.-Y. Wang, S.-C. Yuan and J. Pei, *Angew. Chem., Int. Ed.*, 2013, **52**, 3117–3120.
39 X. Wang, Q. Liao, H. Li, S. Bai, Y. Wu, X. Lu, H. Hu, Q. Shi and H. Fu, *J. Am. Chem. Soc.*, 2015, **137**, 9289–9295.
40 A. Shao, Y. Xie, S. Zhu, Z. Guo, S. Zhu, J. Guo, P. Shi, T. D. James, H. Tian and W. H. Zhu, *Angew. Chem., Int. Ed.*, 2015, **54**, 7275–7280.
41 E. Arbaciauskiene, K. Kazlauskas, A. Miasojedovas, S. Jursenas, V. Jankauskas, W. Holzer, V. Getautis and A. Sackus, *Synth. Met.*, 2010, **160**, 490–498.
42 X.-Y. Wang, F.-D. Zhuang, R.-B. Wang, X.-C. Wang, X.-Y. Cao, J.-Y. Wang and J. Pei, *J. Am. Chem. Soc.*, 2014, **136**, 3764–3767.
43 Z. Zhong, X.-Y. Wang, F.-D. Zhuang, N. Ai, J. Wang, J.-Y. Wang, J. Pei, J. Peng and Y. Cao, *J. Mater. Chem. A*, 2016, **4**, 15420–15425.
44 Y. Fu, K. Zhang, E. Dmitrieva, F. Liu, J. Ma, J. J. Weigand, A. A. Popov, R. Berger, W. Pisula, J. Liu and X. Feng, *Org. Lett.*, 2019, **21**, 1354–1358.
45 H. Fukagawa, T. Oono, Y. Iwasaki, T. Hatakeyama and T. Shimizu, *Mater. Chem. Front.*, 2018, **2**, 704–709.
46 P. Qiang, Z. Sun, M. Wan, X. Wang, P. Thiruvengadam, C. Bingi, W. Wei, W. Zhu, D. Wu and F. Zhang, *Org. Lett.*, 2019, **21**, 4575–4579.
47 N. Gao, C. Cheng, C. Yu, E. Hao, S. Wang, J. Wang, Y. Wei, X. Mu and L. Jiao, *Dalton Trans.*, 2014, **43**, 7121–7127.
48 X.-Y. Wang, F.-D. Zhuang, X. Zhou, D.-C. Yang, J.-Y. Wang and J. Pei, *J. Mater. Chem. C*, 2014, **2**, 8152–8161.
49 T. Hatakeyama, K. Shiren, K. Nakajima, S. Nomura, S. Nakatsuka, K. Kinoshita, J. Ni, Y. Ono and T. Ikuta, *Adv. Mater.*, 2016, **28**, 2777–2781.
50 S. K. Jeon, H. J. Jang and J. Y. Lee, *Adv. Opt. Mater.*, 2019, **7**, 1801462.
51 S. H. Han, J. H. Jeong, J. W. Yoo and J. Y. Lee, *J. Mater. Chem. C*, 2019, **7**, 3082–3089.
52 S. Oda, B. Kawakami, R. Kawasumi, R. Okita and T. Hatakeyama, *Org. Lett.*, 2019, **21**, 9311–9314.
53 X. Liang, Z.-P. Yan, H.-B. Han, Z.-G. Wu, Y.-X. Zheng, H. Meng, J.-L. Zuo and W. Huang, *Angew. Chem., Int. Ed.*, 2018, **57**, 11316–11320.
54 K. Matsui, S. Oda, K. Yoshiura, K. Nakajima, N. Yasuda and T. Hatakeyama, *J. Am. Chem. Soc.*, 2018, **140**, 1195–1198.
55 J. E. Anthony, A. Facchetti, M. Heeney, S. R. Marder and X. Zhan, *Adv. Mater.*, 2010, **22**, 3876–3892.
56 X. Zhan, Z. Tan, B. Domercq, Z. An, X. Zhang, S. Barlow, Y. Li, D. Zhu, B. Kippelen and S. R. Marder, *J. Am. Chem. Soc.*, 2007, **129**, 7246–7247.
57 B. J. Jung, N. J. Tremblay, M.-L. Yeh and H. E. Katz, *Chem. Mater.*, 2011, **23**, 568–582.
58 B. A. Jones, M. J. Ahrens, M.-H. Yoon, A. Facchetti, T. J. Marks and M. R. Wasielewski, *Angew. Chem., Int. Ed.*, 2004, **43**, 6363–6366.
59 S. He, J. Liu, G. Yang, Z. Bin and J. You, *Mater. Horizons*, 2022, **9**, 2818–2823.
60 J. Hoffmann, B. Geffroy, E. Jaques, M. Hissler and A. Staubitz, *J. Mater. Chem. C*, 2021, **9**, 14720–14729.
61 G. Turkoglu, M. E. Cinar and T. Ozturk, *Molecules*, 2017, **22**, 1522.
62 K. R. Naveen, H. I. Yang and J. H. Kwon, *Commun. Chem.*, 2022, **5**, 149.
63 J. M. Ha, S. H. Hur, A. Pathak, J.-E. Jeong and H. Y. Woo, *NPG Asia Mater.*, 2021, **13**, 53.
64 S. K. Mellerup and S. Wang, *Trends Chem.*, 2019, **1**, 77–89.
65 H. Ito, K. Yumura and K. Saigo, *Org. Lett.*, 2010, **12**, 3386–3389.
66 H. Lee, M. Fischer, B. K. Shoichet and S.-Y. Liu, *J. Am. Chem. Soc.*, 2016, **138**, 12021–12024.
67 L. Liu, A. J. V. Marwitz, B. W. Matthews and S.-Y. Liu, *Angew. Chem., Int. Ed.*, 2009, **48**, 6817–6819.
68 P. G. Campbell, A. J. V. Marwitz and S. Y. Liu, *Angew. Chem., Int. Ed.*, 2012, **51**, 6074–6092.

69 H. Huang, L. Liu, J. Wang, Y. Zhou, H. Hu, X. Ye, G. Liu, Z. Xu, H. Xu, W. Yang, Y. Wang, Y. Peng, P. Yang, J. Sun, P. Yan, X. Cao and B. Z. Tang, *Chem. Sci.*, 2022, **13**, 3129–3139.
70 Y. Chen, W. Chen, Y. Qiao, X. Lu and G. Zhou, *Angew. Chem., Int. Ed.*, 2020, **59**, 7122–7130.
71 C. Zhang, L. Zhang, C. Sun, W. Sun and X. Liu, *Org. Lett.*, 2019, **21**, 3476–3480.
72 Y. Zhang, C. Zhang, Y. Guo, J. Ye, B. Zhen, Y. Chen and X. Liu, *J. Org. Chem.*, 2021, **86**, 6322–6330.
73 L. Zi, J. Zhang, C. Li, Y. Qu, B. Zhen, X. Liu and L. Zhang, *Org. Lett.*, 2020, **22**, 1499–1503.
74 C. Li, Y. Liu, Z. Sun, J. Zhang, M. Liu, C. Zhang, Q. Zhang, H. Wang and X. Liu, *Org. Lett.*, 2018, **20**, 2806–2810.
75 Q. Zhang, Z. Sun, L. Zhang, M. Li, L. Zi, Z. Liu, B. Zhen, W. Sun and X. Liu, *J. Org. Chem.*, 2020, **85**, 7877–7883.
76 J. Luo, Z. Xie, J. W. Y. Lam, L. Cheng, B. Z. Tang, H. Chen, C. Qiu, H. S. Kwok, X. Zhan and Y. Liu, *Chem. Commun.*, 2001, 1740–1741.
77 S. Suzuki, S. Sasaki, A. S. Sairi, R. Iwai, B. Z. Tang and G. Konishi, *Angew. Chem., Int. Ed.*, 2020, **59**, 9856–9867.
78 G. Dormán, H. Nakamura, A. Pulsipher and G. D. Prestwich, *Chem. Rev.*, 2016, **116**, 15284–15398.
79 F. Würthner, *Angew. Chem., Int. Ed.*, 2020, **59**, 14192–14196.
80 P. Liao, J. Huang, Y. Yan and B. Z. Tang, *Mater. Chem. Front.*, 2021, **5**, 6693–6717.
81 H. Wang, E. Zhao, J. W. Y. Lam and B. Z. Tang, *Mater. Today*, 2015, **18**, 365–377.
82 F. Ye, C. Shen, J. Guan, Y. Liu, X. Wang, J. Wang, M. Cong, W. Wang, T. Zhang, B. Zou, J. Zheng and Y. Ma, *J. Mater. Chem. C*, 2022, **10**, 3560–3566.
83 W.-M. Wan, D. Tian, Y.-N. Jing, X.-Y. Zhang, W. Wu, H. Ren and H.-L. Bao, *Angew. Chem., Int. Ed.*, 2018, **57**, 15510–15516.
84 A. J. V. Marwitz, A. N. Lamm, L. N. Zakharov, M. Vasiliu, D. A. Dixon and S.-Y. Liu, *Chem. Sci.*, 2012, **3**, 825–829.
85 T. Taniguchi and S. Yamaguchi, *Organometallics*, 2010, **29**, 5732–5735.
86 A. Kundu, S. Karthikeyan, Y. Sagara, D. Moon and S. P. Anthony, *Phys. Chem. Chem. Phys.*, 2018, **20**, 27385–27393.
87 G. Wiethaus, J. M. Toldo, F. da Silveira Santos, R. da Costa Duarte, P. F. B. Gonçalves and F. S. Rodembusch, *Phys. Chem. Chem. Phys.*, 2019, **21**, 4408–4420.
88 S. Kagatikar and D. Sunil, *J. Mater. Sci.*, 2022, **57**, 105–139.
89 L. Xiao, Z. Chen, B. Qu, J. Luo, S. Kong, Q. Gong and J. Kido, *Adv. Mater.*, 2011, **23**, 926–952.
90 H. Sasabe and J. Kido, *J. Mater. Chem. C*, 2013, **1**, 1699–1707.
91 C. Fan and C. Yang, *Chem. Soc. Rev.*, 2014, **43**, 6439–6469.
92 C. Murawski, K. Leo and M. C. Gather, *Adv. Mater.*, 2013, **25**, 6801–6827.
93 S. Schmidbauer, A. Hohenleutner and B. König, *Adv. Mater.*, 2013, **25**, 2114–2129.
94 Y. Chen and D. Ma, *J. Mater. Chem.*, 2012, **22**, 18718–18734.
95 S. J. Blanksby and G. B. Ellison, *Acc. Chem. Res.*, 2003, **36**, 255–263.
96 D. J. Grant and D. A. Dixon, *J. Phys. Chem. A*, 2006, **110**, 12955–12962.
97 M. Sugie, H. Takeo and C. Matsumura, *Chem. Phys. Lett.*, 1979, **64**, 573–575.
98 C. Hansch, A. Leo and R. W. Taft, *Chem. Rev.*, 1991, **91**, 165–195.
99 A. Dreuw and M. Head-Gordon, *J. Am. Chem. Soc.*, 2004, **126**, 4007–4016.
100 T. Yanai, D. P. Tew and N. C. Handy, *Chem. Phys. Lett.*, 2004, **393**, 51–57.
101 J.-D. Chai and M. Head-Gordon, *Phys. Chem. Chem. Phys.*, 2008, **10**, 6615–6620.
102 B. Sadowski, M. Kaliszewska, Y. M. Poronik, M. Czichy, P. Janasik, M. Banasiewicz, D. Mierzwa, W. Gadomski, T. D. Lohrey, J. A. Clark, M. Łapkowski, B. Kozankiewicz, V. I. Vullev, A. L. Sobolewski, P. Piatkowski and D. T. Gryko, *Chem. Sci.*, 2021, **12**, 14039–14049.